Eur. Phys. J. B **43**, 19–27 (2005)
DOI: 10.1140/epjb/e2005-00023-9

THE EUROPEAN PHYSICAL JOURNAL B

Hydrogen desorption from ball milled MgH_2 catalyzed with Fe

A. Bassetti[1], E. Bonetti[1], L. Pasquini[1,a], A. Montone[2], J. Grbovic[2,b], and M. Vittori Antisari[2]

[1] Department of Physics, University of Bologna and INFM, Bologna, Italy
[2] Materials and Technology Unit, ENEA C.R. Casaccia, Roma, Italy

Received 5 October 2004 / Received in final form 23 November 2004
Published online 11 February 2005 –

Abstract. In order to obtain faster hydrogen sorption kinetics, MgH_2-Fe nanocomposites were prepared by high-energy ball milling. The MgH_2 decomposition was studied in samples obtained by changing in a systematic way both the catalyst amount and the degree of microstructural refinement. To this purpose, blends containing increasing Fe concentration have been ball milled in processing conditions able to impart different amount of structural defects. The resulting samples have been characterized by X-ray diffraction to investigate the microstructural features and the phase composition, while the powder morphology and the degree of catalyst dispersion were analyzed by scanning electron microscopy. Differential scanning calorimetry was carried out to characterize the hydrogen desorption behavior of these nanocomposites. Experimental results clearly show that the characteristics of the desorption process are dominated, among other factors, by the morphology of the catalyst dispersion, which in turns depends on the processing conditions and blend composition. In order to achieve low desorption temperatures the homogeneous catalyst dispersion in micron-size particles throughout the structure is required. This condition can be achieved by suitable tuning of the milling conditions and of the catalyst amount.

PACS. 61.72.-y Defects and impurities in crystals; microstructure – 64.70.Hz Solid-vapor transitions – 66.30.Pa Diffusion in nanoscale solids – 81.07.Bc Nanocrystalline materials

1 Introduction

Metal hydrides have been recently the subject of intensive research activities owing to their potential application for high capacity hydrogen storage. Among the most important parameters for this kind of technological application, a key role is played by the storage capacity, both in mass and volume; moreover also the kinetics of hydride decomposition, and in particular the rate of hydrogen desorption versus temperature is an important feature. As far as the storage capacity is concerned, a noticeable research effort is devoted to light metallic elements and in particular to Mg which is able to store 7.6 wt% of hydrogen in the stoichiometric hydride MgH_2. A further interesting feature of this material, whose hydride can be synthesized by solid state reaction of Mg with H_2 gas, is the reversible hydrogen adsorption and desorption, a mandatory feature for the technological applications requiring often a large number of charge-discharge cycles. However, among others, some critical aspects for the technological exploitation of Mg based materials are related to the strong interaction of Mg with hydrogen, which is reflected by the relatively high desorption temperature. Furthermore the transport of hydrogen, both at the surface and in the bulk are relatively poor so that a sluggish reactions between Mg and hydrogen gas is often observed. Both effects contribute to imposing a operating temperature too high in order to be compatible with the operating features of the polymer electrolyte fuel cells so that materials with faster kinetics at lower temperature are expected as result of a research effort. The processing route explored by most researchers concerns microstructural modifications able to assist the hydrogen release.

Mechanical alloying (MA) is a well-established method for processing metallic powders, able to impart a high density of crystal defects, which can, among other effects, improve the mass transport and diffusion properties of a metallic material. Moreover this method can be used to synthesize nanostructured alloys and intermetallic compounds, including metal hydrides, by interdiffusion reactions in the solid state [1,2]. In the case of MgH_2 it has been proved that the reduction of the crystallite size down to the nanometer range by ball milling processing can significantly improve the H transport properties and the hydrogenation and dehydrogenation kinetics. The ball milling processing of both Mg and MgH_2 has been consequently the subject of several papers aiming to improve

[a] e-mail: luca.pasquini@bo.infm.it
[b] *Permanent address*: INN Vinca Dep. of Material Science, Belgrade, Serbia and Montenegro

the reaction kinetics without reducing the hydrogen storage capacity [3–5].

Ball milling can be also useful for adding to the Mg compounds small amounts of catalyst able to assist the hydrogenation and dehydrogenation reaction. In fact the difficulty of the metallic Mg in assisting the dissociation/recombination of the H_2 molecule is well ascertained.

In conclusion ball milling processing can be so used to impart structural refinement and to disperse a suitable catalyst in a single operation. However each single process is expected to proceed with its own kinetics so that the processing route has to be optimized taking into account both elementary effects. The problem can be further complicated by possible reciprocal interactions between structural refinement and catalyst dispersion.

The catalytic effect of most 3d-transition metals like Ti, V, Mn, Fe, Co, Ni [5,6] and of most of their oxides [7] has been proved. Furthermore also hydride forming intermetallic compounds with low hydrogen desorption temperature, like $LaNi_5$, $FeTi_{1.2}$, $ZrFe_{1.4}Cr_{0.6}$ [8–11], have been shown to be effective to the purpose. In most cases a significant improvement of the hydrogenation and dehydrogenation kinetics has been reported even if the results often depended on the details of the processing route [12] so that the description of the desorption process is not already well established.

The purpose of the present paper is to further investigate this point. In particular our aim is to explore the combined effect of the microstructural refinement and of the amount of catalyst on the H desorption kinetics.

In fact, the MgH_2 decomposition and the related hydrogen desorption process comprises probably several elementary steps, among which the H transport through the hosting matrix, affected by the microstructural refinement, and the dissociation/recombination rate of molecular H_2 at the surface, influenced by the presence of catalytic particles, can play a major role. The rate limiting step of the macroscopic H desorption process is probably related to the features of both processes and our aim is then to better understand this point.

From the experimental point of view, MgH_2 and Fe have been chosen as a model system on the basis of the literature results showing how the Fe addition is able to strongly affect the H_{gas}-Mg interaction [13,14]. The degree of microstructural refinement of the MgH_2 crystal and the amount of Fe catalyst have been systematically changed, in order to check for possible correlations between these two parameters and the H desorption kinetics. The microstructural refinement of MgH_2 has been modulated by changing the ball to powder ratio in the ball milling process. In fact, this parameter is known to affect the amount of energy imparted to the powder particles [15], which in turns gives rise to a different amount of stable structural defects.

The microstructure of the processed powders has been systematically characterized by X-ray diffraction, supported by Rietveld analysis, while morphological features have been analyzed by Scanning Electron Microscopy; the H desorption behavior has been evaluated by Differential Scanning Calorimetry.

2 Experimental

Magnesium hydride MgH_2, (60 μm particle size, containing 5 wt.% Mg as impurity, from Th. Goldmischmidt) and Fe (Alfa, 99,998%) powders were processed by ball milling in a Spex Mixer/Mill 8000. All samples have been processed for a fixed time of 10 hours under 2 bar Ar atmosphere using specially designed hardened steel vials equipped with a needle valve (Cantil Srl, `http://www.cantil.it`) allowing evacuation and gas filling.

Since the purpose of the work is to explore the combined effect of the milling intensity and of the amount of catalyzing element on the desorption properties of MgH_2, both parameters have been changed in a systematic way, giving rise to a grid of samples covering a quite wide range of experimental situations. The milling intensity has been adjusted by changing the ball to powder ratio (BPR), while keeping constant the remaining parameters. The BPR has been set to 1:1, 3:1, 10:1 and 20:1; to this purpose the amount of processed powder has been kept constant in all experiments, while the ball weight has been adjusted to the required value for each sample. Furthermore, the Fe concentration values which have been explored are 2 wt.%, 5 wt.%, 10 wt.% and 20 wt.%. Each sample in the following is then identified by two features, the first being related to the BPR and the second to the Fe content.

The microstructure of the powders was characterized by X-ray diffraction (XRD) with a Rigaku-DMAX IIIC Bragg-Brentano diffractometer, equipped with Cu-Kα radiation and a graphite monochromator in the diffracted beam.

The Rietveld analysis of the XRD profiles has been performed by the MAUD package [16], to evaluate the average crystallite size d, the microstrain $\langle \varepsilon^2 \rangle^{1/2}$ and the relative amount of the different phases.

Morphological and microanalytical characterization was carried out by Scanning Electron Microscopy (SEM) with a Cambridge 250MKIII equipped with EDS microanalysis and backscattered electron detector. To evaluate the particle size distribution, the as milled powders were sonicated in ethanol for 15 minutes and then a drop of the suspension was allowed to dry on a carbon tape. The particle size distribution was evaluated by analysing the digital micrographs with the software package ImageJ (`http://rsb.info.nih.gov/ij/`).

Moreover, in order to investigate the sample homogeneity and the catalyst dispersion, backscattered electron images, sensitive to the local chemical composition, have been taken on flat polished sections, obtained by embedding the powder in epoxy resin followed by the usual metallographic preparation of the resulting composite. A thin carbon coating was vacuum deposited before the SEM observation.

Finally hydrogen desorption was investigated by differential scanning calorimetry (DSC) using a DSC2010

Table 1. Phase composition (wt.%) in as-milled samples determined from Rietveld analysis of XRD profiles.

Sample	MgH_2 (wt%)	γ-MgH_2 (wt%)	MgO (wt%)	Mg (wt%)	Fe (wt%)	Mg_2FeH_6 (wt%)
1:1−10 wt%	66	22	4.5	2.5	5	–
1:1−5 wt%	67	23	5	3	2	–
1:1–2 wt%	68	23	5	2	1	–
3:1–10 wt%	63	26	4	–	7	–
3:1–5 wt%	62	26	5.5	3	3.5	–
3:1–2 wt%	66.5	25	4	3.5	1	–
10:1–10 wt%	50	29	8	4	9	–
10:1–5 wt%	58	30	5.5	2	4.5	–
10:1–2 wt%	57	36	6	–	1	–
20:1–10 wt%	52	32.5	6	–	9	1
20:1–5 wt%	57	31	7.5	–	4	0.5

Table 2. Crystallite size and microstrain in as-milled samples determined from Rietveld analysis of XRD profiles.

Sample	MgH_2		γ-MgH_2		MgO		Fe	
	d (nm)	$\langle\varepsilon^2\rangle^{1/2}$	d (nm)	$\langle\varepsilon^2\rangle^{1/2}$	d (nm)	$\langle\varepsilon^2\rangle^{1/2}$	d (nm)	$\langle\varepsilon^2\rangle^{1/2}$
1:1–10 wt%	7.2	0.6	3.4	0.5	7.6	3	81.0	0.3
1:1–5 wt%	7.7	0.7	3.9	0.1	3.5	1	85.0	0.3
1:1–2 wt%	8.3	0.5	3.3	0.1	3.9	0.2	115	0.3
3:1–10 wt%	5.3	0.3	4.8	0.2	5.0	3	51.0	0.3
3:1–5 wt%	5.5	0.6	5.2	0.1	3.7	1	66.0	0.4
3:1–2 wt%	5.8	0.5	5.0	0.1	4.1	1	65.0	0.3
10:1–10 wt%	4.8	0.5	3.8	0.2	3.4	2	30.0	0.5
10:1–5 wt%	5.3	0.1	5.3	0.07	5.0	2.5	31.0	0.4
10:1–2 wt%	5.0	0.4	4.3	0.5	6.0	2	59.0	0.5
20:1–10 wt%	4.9	0.3	5.0	0.6	5.0	4	18.0	0.4
20:1–5 wt%	4.4	0.5	4.0	0.6	3.5	1	21.0	0.5

(TA Instruments) under 99.9995% pure Ar flow with Cu crucibles. Heating runs at a fixed heating rate of 20 K/min as well as isothermal treatments were carried out.

3 Results

3.1 XRD characterization

Figure 1 shows XRD profiles for the as-milled samples having the same Fe concentration C_{Fe} = 10 wt.% processed with different values of the BPR, ranging from 20:1 to 1:1.

From the results of Rietveld refinement on the complete set of samples, reported in Tables 1 and 2, it is possible to evaluate the effect of the milling energy and the one of the Fe concentration on the final microstructure, whose main features are discussed in the following.

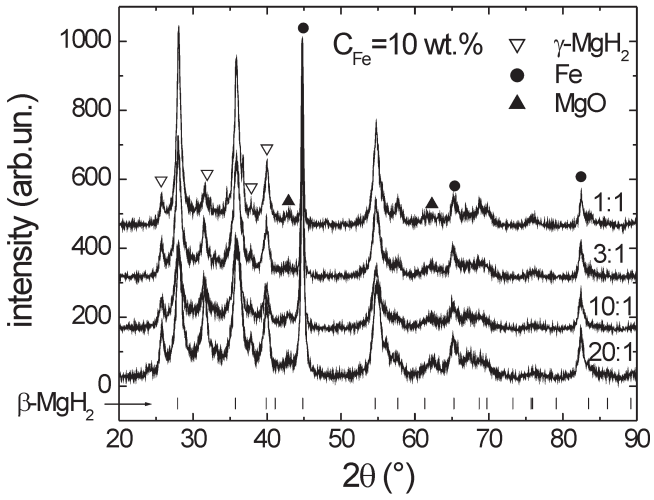

Fig. 1. XRD profiles of as-milled samples processed with different BPR values with the same C_{Fe} = 10 wt.%.

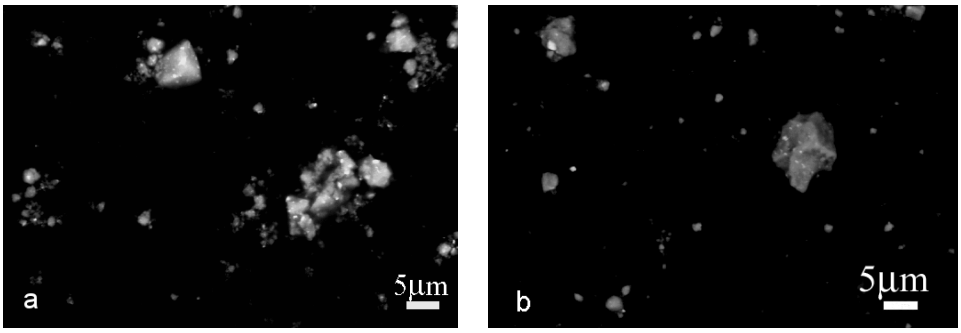

Fig. 2. BSE images of samples: a) 10:1−10 wt.%; b) 10:1−5 wt.%.

The crystallites of tetragonal β-MgH_2, whose size in the unprocessed material is larger than 100 nm, which represents the sensitivity of our diffractometer, are fragmented down to the nanometric range in whichever explored conditions. The resulting crystallite size depends on the BPR and it ranges from 7−8 nm at low energy to 4−5 nm at high energy of miling, independently on the Fe content which does not affects the crystallite refinement in a detectable way.

As far as the Fe crystallite size is concerned, we observe a similar behavior. In fact, also in this case the ball milling induces nanometric crystallites with a size gradually decreasing from 81 nm down to 18 nm by increasing BPR. It has to be noticed that smaller Fe crystallites are observed when the Fe content is higher, for every value of BPR. Also the microstrain introduced in the Fe lattice slowly increases with the BPR.

In the samples milled at low BPR, the Rietveld analysis invariably underestimates the Fe content. This effect can be ascribed to a rough Fe particle dispersion in the hydride phase in these processing conditions. In fact, when a large grained two phase material is examined by X-ray diffraction, the relative intensities scattered by the two phases can be affected by the morphological details of the composite and are not anymore depending only on the relative phase amount, beyond the scattering features. The effect is particularly evident in presence of a large asymmetry between the absorption length of the X radiation in the two phases. This is typically our case, since the absorption length of Cu-Kα is much smaller in bcc Fe ($\approx$10 μm) than in MgH_2. Only when the microstructure is finely interdispersed on the scale of the shorter absorption length the hypothesis at the basis of the Rietveld algorithms are fulfilled and a reliable determination of the minority phase content on the basis of the scattered intensities can be obtained. We will show later how this interpretation can be supported by the SEM observations.

The ball milling process induces a phase transformation from β-MgH_2 to orthorhombic γ-MgH_2 whose abundance increases with BPR. Since γ-MgH_2 can be considered as a distortion of β-MgH_2 (it exhibits the same packing type and coordination number), this observation can support the results relative to the microstrain and so to the lattice distortion which gradually increases with the milling energy. Also in this case the Fe content plays a minor role.

For very high milling intensity, when the BPR = 20:1 a small amount of ternary phase Mg_2FeH_6 is detected. The formation of Mg_2FeH_6 by ball milling MgH_2 and Fe has been already reported [17]; here it was not taken into account in the following, owing to its negligible amount.

Finally, we want to observe that the concentration of MgO is limited to about 5 wt.%. This feature can be considered quite satisfactory considering the high oxidation potential of Mg and appears related mainly to the oxidation of the metallic Mg present as impurity in the starting material.

In conclusion, from the analysis of the X-ray diffraction spectra, it is possible to see how the BPR is a suitable parameter to affect the degree of microstructural refinement of ball milled mixtures of MgH_2 and Fe. In particular, the size of the coherent domains of both phases is gradually reduced by increasing the ball milling energy, indicating that the process is really effective in reducing the scale length of the sample microstructure. The Fe content does not affect the microstructure in a relevant way so that it is possible to consider the structural refinement of the MgH_2 matrix and the Fe dispersion to be independent from eachother even if they occur during the same process.

3.2 SEM observations

Figure 2 shows back-scattered electron (BSE) images of the as-milled powder, with BPR 10:1 and Fe content 10 and 5%, not subjected to any particular specimen preparation procedure. Rather small particles, a few μm in size can be observed together with larger entities having lateral dimension larger than 50 μm. Higher magnification observations show that these last particles are actually formed by the agglomerations of smaller particles, which often exhibit platelet-like shape.

In order to give reliable and repeatable results on the measurement of the average particle size, the specimens for the SEM observation have been prepared by sonicating the powder in ethanol in order to disaggregate the elementary powder grains. Residual agglomerates still present in the sample were not taken into account in the particle counting, so that the result is expected to be representative of the size of the elementary powder particles, while

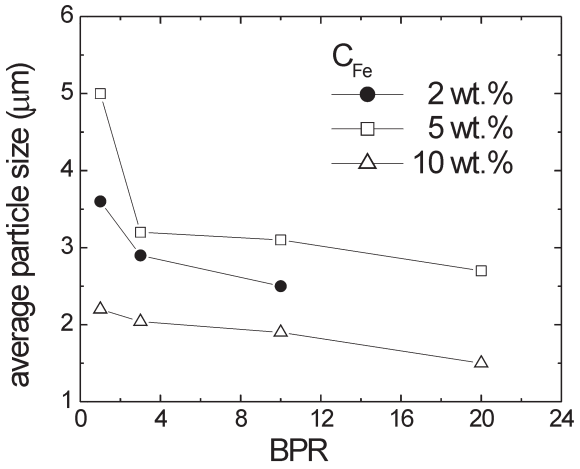

Fig. 3. Average particle size determined from SEM analysis on as-milled samples, for different Fe concentrations C_{Fe} and as a function of the ball-to-powder-ratio (BPR).

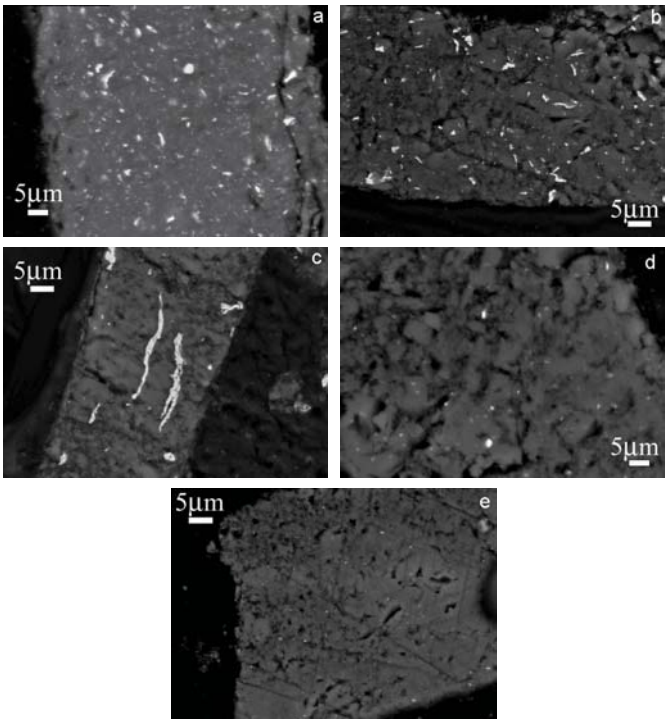

Fig. 4. BSE images showing the morphology of catalyst dispersion (white spots are Fe) for samples processed under different conditions. a) 10:1−10 wt.%; b) 3:1−10 wt.%; c) 1:1−10 wt.%; d) 10:1−2 wt.%; e) 20:1−10 wt.%.

no information are provided on their agglomeration status in the as milled conditions. The average particle size has been obtained by digitally processing the SEM images and at least 500 particles have been taken into account for each average size determination.

The average particle size versus the BPR, for different Fe contents is reported in Figure 3, where it is possible to observe the considerable morphological refinement of the 60 μm starting powders in whichever combination of the experimental parameters. Besides this macroscopic effect, the average particle size shows a fable dependence on milling intensity and the Fe content. In fact, both a high milling energy and a high Fe content generally enhance the morphological refinement, so that smaller powder particles are obtained by milling at the higher BPR the mixture containing a large enough amount of Fe.

The effect of the milling parameters is much more evident as far as the compositional homogeneity of the samples is concerned. In fact, it is possible to observe how size, shape and degree of dispersion of Fe particles in the hydride matrix are deeply affected by the processing parameters as shown in the backscattered electron images of Figure 4 where the white dots correspond to the heavier Fe particles. Only for high milling intensity and a large enough amount of Fe in the blend, a fairly uniform distribution of Fe particles with a size in the range 2−5 μm dispersed in the hydride matrix can be observed. This can be seen in Figure 4a where the image relative to the sample with C_{Fe} = 10 wt.% processed with BPR = 10:1 is reported.

Larger Fe particles are instead overwhelming in Figure 4b, where BPR = 3:1. A further decrease of BPR down to 1:1 leads to a reduced Fe fragmentation so that large, elongated Fe particles with a length larger than 10−15 microns can be observed in Figure 4c.

The uniform dispersion of Fe particles is related, besides the BPR, also to Fe content of the mixture. In fact, when C_{Fe} is small, the Fe dispersion never appears uniform, so that rather large sample regions free from Fe particles can be observed, as reported in Figure 4d.

From the morphological and microanalytical observation it is possible to conclude that the most evident effect related to the milling intensity and to the Fe content is found on the refinement of the Fe particles and on their uniform dispersion inside the matrix. In fact, while a strong refinement of the 60 μm Mg hydride particle is observed for all the processing conditions, so that all the milled samples show particle sizes and surface areas of the same order of magnitude, the refinement and dispersion of the Fe particles is much more sensitive to the processing conditions. It is observed to evolve from large particles with inhomogeneous distribution at low values of the milling energy and of the Fe concentration, to a nice uniform dispersion of small particles for proper processing parameters, when a sufficiently Fe rich mixture is ball milled with a high value of BPR.

Under the hypothesis that the Fe can act as a catalyzing agent for the MgH_2 decomposition reaction, so that the atomic hydrogen has to migrate to the Fe particle in order to be released, the above results appear quite relevant. In this frame, the surface density of desorption sites as well as the average inter-particle distance defining in some way an effective diffusion length can play a major role on the kinetics of the reaction.

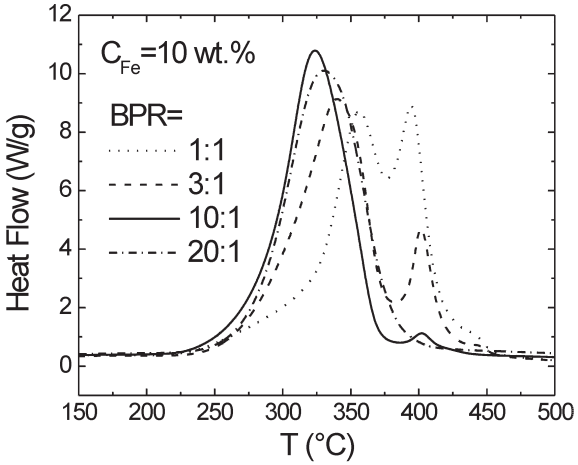

Fig. 5. DSC runs for samples with the same C_{Fe} = 10 wt.% and different BPR values. Experiments carried out at 20 K/min, under 1 bar of 99.9995% pure Ar flowing at 40 cm^3/min.

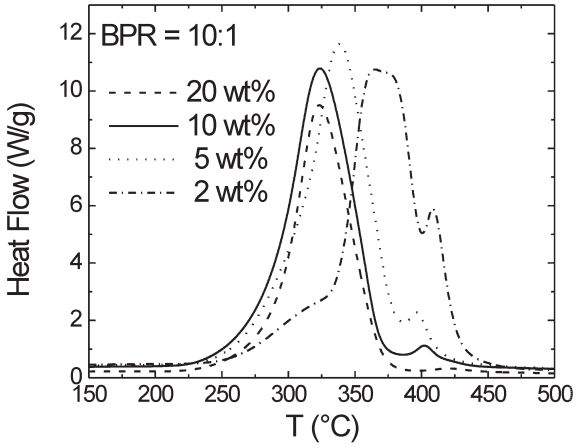

Fig. 6. DSC for samples with the same BPR = 10:1 and different C_{Fe} values. Experiments carried out at 20 K/min, under 1 bar of 99.9995% pure Ar flowing at 40 cm^3/min.

3.3 DSC investigations

Figure 5 shows the influence of different milling energy on the features of H-desorption from samples having the same Fe content of 10 wt%, as resulting from DSC heating runs performed at 20 K/min; in Figure 6 the effect of Fe content, all the other parameters being constant, is instead reported.

The DSC traces suggest a complex desorption behavior, generally characterized by more than one single peak. In particular, it is possible to identify two main features, a combination of which, with different relative weights, can describe at a first approximation all the DSC traces. The first is a relatively sharp peak with roughly constant FWHM, located at about 400 °C, while the second is a broader peak present between about 220 °C and about 400 °C, whose FWHM and peak position are more deeply affected by the processing conditions.

It has to be noticed that the sharp peak around 400 °C corresponds quite nicely to the decomposition of non catalyzed and ball milled MgH_2 [18]. The straightforward interpretation of the DSC traces can consider, at the first approximation, the following steps. As experimentally evident, the decomposition begins, always at same temperature of about 220 °C, probably at the Fe-MgH_2 interface where the metallic Fe catalyzes the decomposition reaction. Increasing the temperature, the surface density of the Fe particles and their average interparticle distance are probably the main parameters affecting the desorption rate since they control the density of desorption sites and the average H diffusion length to the desorption site. The change in width and position of the low temperature peak can so reflect the different microstructural refinement induced by the different ball milling processing conditions. Furthermore, the relatively large width of this low temperature peak can be probably ascribed to the stochastic nature of the ball milling process, so that a quite broad range of local microstructural situations can be present in the same sample.

Table 3. Normalized areas A_n and peak temperatures T_P of the endothermic H-desorption process measured in DSC heating runs.

Sample	A_n	T_P (°C)
MgH_2 – ref.	1	447
1:1–10 wt%	0.958	394
1:1–5 wt%	0.975	406
1:1–2 wt%	0.991	410
3:1–10 wt%	0.899	339
3:1–5 wt%	0.946	354
3:1–2 wt%	0.988	400
10:1–20 wt%	0.649	323
10:1–10 wt%	0.833	324
10:1–5 wt%	0.952	338
10:1–2 wt%	0.983	365
20:1–10 wt%	0.865	330
20:1–5 wt%	0.906	367

A further temperature increase induces the non catalyzed decomposition of the base material, so that all the hydride remaining after the thermal history decomposes at the same temperature of about 400 °C. The corresponding reaction appears to be quite fast considering the sharpness of the corresponding endothermic peak, and this can be probably explained by the fact that no peculiar surface sites are required for the decomposition reaction at this temperature, but the whole surface is active in the process. Moreover the small shifts in the peak temperature can be due do the different structural refinements among different samples, since both defect density and average particle size can, in principle, affect this desorption temperature.

The total area under the endothermic desorption peaks, once normalized to the one measured on the unprocessed commercial hydride under the same conditions, is reported in Table 3 as A_n, where also the temperature T_P corresponding to the highest peak in the thermogram is reported. A_n is of course proportional to the hydride content of the mixture through the hydride decomposition heat. Assuming that none effect is related to the presence of Fe and that no appreciable change in the decomposition heat of the system is induced by ball milling, as demonstrated by pressure-composition-temperature isotherms on similar materials [19], we can consider A_n as a reliable estimation of the hydride weight fraction in each sample. This value is indeed in good agreement with the hydride weight fraction derived from Rietveld analysis. It is worth mentioning that XRD performed on samples decomposed by DSC runs did not reveal any trace of residual hydride.

Noteworthy is the reduction of T_P by about 120 °C with respect to the reference hydride achieved in samples rich in Fe and processed with high values of BPR, which keeps A_n above 0.8.

Desorption kinetics were also investigated by means of DSC isotherms. The integrated calorimetric signal $A_{iso}(t)$ was converted into the gravimetric hydrogen capacity $C_H(t)$ using the equation:

$$C_H(t) = 7.22 \times (A_n - A_{iso}(t)/A_{ref})$$

where $7.22 = 0.95 \times 7.6$ represents the nominal hydrogen capacity (wt.%) of 95% pure MgH_2. Figure 7 shows $C_H(t)$ versus time at different temperatures for the sample 10:1−10 wt.%. For comparison purposes we report also the curves relative to unprocessed MgH_2 and to the sample 10:1−2 wt.%. The unprocessed hydride shows a very slow kinetics even at 300 °C. The proper combination of Fe addition and ball milling parameters for optimum microstructure leads to a significant fastening of the desorption kinetics, so that almost the whole H content can be released in less than 10^3 seconds at 300 °C. For intermediate situations, like for an amount of Fe of 2 wt.%, the microstructure is not suitable for a fast reaction even after processing at high energy, so a much slower decomposition of the hydride is observed, even if, of course, the average gravimetric capacity is higher owing to a larger fraction of MgH_2.

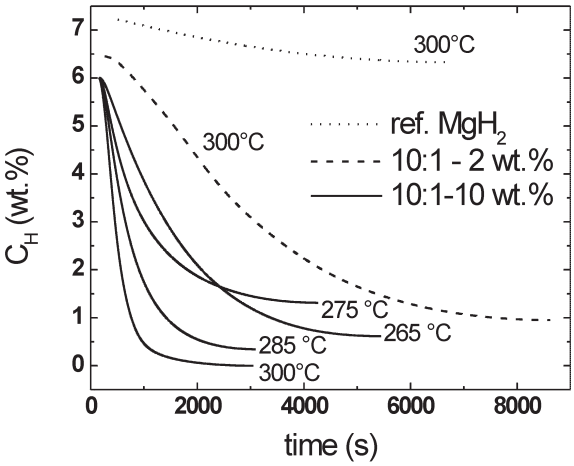

Fig. 7. Gravimetric hydrogen capacity as a function of time derived from DSC isotherms.

4 Discussion

The combined analysis of XRD results and SEM observations can describe in a suitable way the main effects induced by a ball milling process on the mixture of Fe and MgH_2. The energy imparted by the ball milling device to the powder particles as well as the Fe content of the mixture affect different aspects of the composite microstructure, both in terms of lattice distortion and of morphological homogeneity. As usual the description of the microstructural features is a key point for the interpretation of the desorption behavior and for setting up guidelines for its optimization. Based on a schematic frame, the main factors that are expected to influence H-desorption kinetics are, among others, the crystallite size d, the powder particle size, and the catalyst concentration and dispersion.

In fact, at first approximation the crystallite size can be considered to scale inversely with the fraction of internal interfaces, like grain or cell boundaries, or, more generally with the density of structural defects. Since diffusion of small atoms like H is generally faster at the interfaces or at defects than in the perfect lattice, the reduction of the optically coherent zones down to the nm range can increase the effective diffusion coefficient and so the transport properties at fixed temperature. Moreover, the interfaces or defects can probably play a role also in the phase transformation from hydride to metallic Mg, acting as heterogeneous nucleation centers. This point is in principle very important owing to the large metal/hydride volume mismatch that contributes to the nucleation barrier.

As far as the particle size is concerned, it is quite evident that the particle radius defines both the surface area available for the hydrogen desorption as well as the average distance that hydrogen has to diffuse in order to reach the surface where the desorption process is expected to occur.

Finally, the catalyst at the powder particle surface is expected to fasten the last step of the desorption process, by assisting the recombination of the atomic hydrogen into the corresponding volatile molecule.

Our results show that the first two parameters are strongly affected by the ball milling inducing noticeable differences relative to the starting hydride. In fact, the particle size is refined from 60 μm to a few μm, and all the milled samples are characterized by very small d values, in the 4−8 nm range. However, the particle and crystallite size differences among the samples, even if processed in heavily different conditions, are relatively small and they are not able to justify the differences observed in their DSC traces.

This leads to the conclusion that variations of both particle and crystallite size in this range are not expected

to be relevant for the optimization of desorption kinetics. It must however be considered that a nanometric crystallite size and a micrometric particle size are essential features required for fast hydrogen desorption, constituting the preliminary requirements for a further optimization. This aspect is generally accepted and it is supported by the improved behavior shown by the ball milled hydride relative to the as received one.

In our case the optimization of the desorption kinetics appears to be governed by the dispersion of the catalyzing particles. The Fe particle dispersion appears to be the main microstructural parameter affected by the processing condition and whose features well correlate with the structure of the DSC decomposition curves.

Before continuing in this discussion, it is necessary to analyze the structure of the DSC decomposition curves, which, in most cases show a double peak structure. The presence of double peaks in the DSC traces was already observed in absorption-desorption cycles from $LaNi_5$ [20] and in the desorption step from magnesium hydride, where it was attributed to sequential decomposition of γ-MgH_2 and β-MgH_2 [4]. The experimental results clearly demonstrate that this is not occurring in our case. In fact, the relative heights of the two peaks do not correlate at all with the relative abundance of the β-MgH_2 and γ-MgH_2 hydride phases; in particular the samples (10:1−20 wt.%) and (10:1−10 wt.%), which exhibit almost one single peak at low temperature, contain about 30 wt.% γ-MgH_2.

In some cases, more than two peaks can be evidenced in the DSC scan (see Fig. 5, BPR = 1:1). It is noteworthy that the most complex DSC curves pertain to samples where SEM analysis reveals the less homogeneous Fe dispersion.

Our results suggest so that the appearance of several peaks in the DSC scan can be coupled with a non-homogeneous dispersion of the Fe catalyst. At low milling energy (e.g., BPR = 1:1 or 3:1), agglomeration of Fe in large particles (Figs. 4b, c) leaves large hydride regions with poor catalyst concentration. These material volumes are expected to suffer a surface recombination-limited kinetics and therefore a degradation of sorption performances. A similar situation can be expected for samples with low C_{Fe}, though now the main reason lies in the insufficient overall Fe content. On these grounds, we can attribute the low temperature peaks in Figure 5 to well catalyzed regions and the high temperature peak to Fe-depleted regions. In fact, in nanocrystalline MgH_2 ball milled without Fe addition, a T_P of about 410 °C was obtained [18], very similar to the high-temperature peak in Figure 5. The shift of the low temperature peak with increasing BPR observed in Figure 5 could reflect a still different degree of Fe dispersion or can be alternatively ascribed to the decreasing average particle size.

As far as the effect of the Fe concentration is concerned, both DSC runs and isothermal decompositions (Fig. 7) confirm that an enormous improvement of desorption kinetics accompanies the increase of C_{Fe} from 2 to 10 wt.% at the expenses of only 0.5 wt.% loss in the gravimetric hydrogen capacity (Fig. 7, Tab. 3). On the other hand, a further catalyst addition (C_{Fe} = 20 wt.%), does not appear to improve the desorption performances, but significantly reduces the peak area and gravimetric capacity (A_n = 0.649, Tab. 3).

It can be concluded that the reaction kinetics is enhanced by catalyst particles finely dispersed in the sample. The optimum amount can be set around 10 wt%, suggesting that below this concentration the reaction is surface controlled by the recombination of atomic hydrogen into the H_2 molecule. The present hypothesis is supported by the analysis of Barkhordarian et al. of H-desorption kinetics in the MgH_2-Nb_2O_5 ball-milled composites [21]. They were able to show that at the temperature of 300 °C, the desorption reaction is surface controlled when the Nb_2O_5 concentrations was below 0.2 mole%, becoming interface controlled for larger concentrations.

For the samples with C_{Fe} = 10 and 20 wt.% we thus suggest that rate-limiting steps other than surface recombination are controlling the reaction kinetics. We can suppose a kinetic limit owing to nucleation and growth processes following Johnson-Mehl-Avrami kinetics, as pointed out recently in MgH_2-C nanocomposites [22]; alternatively, H-diffusivity in the bulk or the stress associated with the hydride-metal phase transformation can limit the kinetics of hydrogen desorption.

A deeper study of this last aspect appears intrinsically limited when using ball milling as the synthesis tool. Ball milling is quite far from a deterministic process where the processing parameters can be separately adjusted. It affects several microstructural features and it seems impossible to modify the defect density of the matrix, which is expected to affect the transport properties, without changing the catalyst dispersion, which has been shown to have a much more important effect on the desorption process. Probably a different method for introducing the catalyst particles, allowing the microstructural refinement and the catalyst dispersion to be varied independently, has to be set up to further investigate the kinetics aspects of the elementary steps leading to the phase transformation between MgH_2 and metallic Mg.

5 Conclusions

We have shown how, by tuning the ball milling energy and catalyst concentration, the microstructure and morphology of MgH_2-Fe nanocomposites can be changed in a way that directly affects the kinetic features of the hydride decomposition and so the desorption process.

In particular, a high milling energy (BPR = 10:1 or 20:1) and a sufficient amount of Fe catalyst are required in order to attain the optimum microstructure showing a homogeneous distribution of micron and submicron-sized Fe particles in the MgH_2 matrix.

Only in this condition the hydride decomposition is characterized by a low temperature single endothermic peak.

The optimum catalyst concentration results around 10 wt.%, since lower values seem to be insufficient to avoid

the presence of poorly catalyzed regions, while higher values do not further improve the kinetic performances, probably because the reaction becomes rate limited by a different process. The only net effect of increasing the catalyst above 10 wt% is a reduction of the hydrogen storage capacity owing to the smaller fraction of MgH_2.

In conclusion we can report that the sample with optimum microstructure, processed with BPR = 10:1 and having $C_{Fe} = 10$ wt.%, can release, under ≈1 bar Ar pressure, about 5 wt.% of hydrogen in about 600 s at 300 °C and in about 3000 s at 265 °C; this represents a dramatic speed-up of kinetics performances relative to the unprocessed MgH_2.

This research was financially supported by the Italian Ministry for University and Research under project FISR-*Sviluppo di sistemi di accumulo di idrogeno in leghe metalliche per veicoli con celle acombustibile.*

References

1. C.C. Koch, O.B. Cavin, C.G. Mckamey, J.O. Scarborough, Appl. Phys. Lett. **43**, 1017 (1983)
2. R.B. Schwarz, W.L. Johnson, Phys. Rev. Lett. **51**, 415 (1983)
3. J. Huot, G. Liang, S. Boily, A. Van Neste, R. Schulz, J. Alloys Comp. **293–295**, 495 (1999)
4. F.C. Gennari, F.J. Castro, G. Urretavizcaya, J. Alloys Comp. **321**, 46 (2001)
5. A. Zaluska, L. Zaluski, J.O. Ström-Olsen, J. Alloys Comp. **288**, 217 (1999)
6. L. Kanoya, M. Hosoe, T. Suzuki, Honda R&D Tech. Rev. **14**, 9 (2002)
7. W. Oelerich, T. Klassen, R. Bormann, J. Alloys Comp. **315**, 237 (2001)
8. M. Terzieva, M. Khrussanova, P. Peshev, J. Alloys Comp. **267**, 235 (1998)
9. G. Liang, J. Huot, S. Boily, A. Van Neste, R. Schulz, J. Alloys Comp. **297**, 261 (2000)
10. G. Liang, E. Wang, S. Fang, J. Alloys Comp. **223**, 111 (1995)
11. P. Wang, A. Wang, H. Zhang, B. Ding, Z. Hu, J. Alloys Comp. **297**, 240 (2000)
12. L. Zaluski, A. Zaluska, J.O. Ström-Olsen, J. Alloys Comp. **253**, 70 (1997)
13. G. Liang, J. Huot, S. Boily, A. Van Neste, R. Schulz, J. Alloys Comp. **292**, 247 (1999)
14. J.-L. Bobet, E. Akiba, Y. Nakamura, B. Darriet, Int. J. Hydrogen Energy **25**, 987 (2000)
15. N. Burgio, A. Iasonna, M. Magini, S. Martelli, F. Padella, Il Nuovo Cimento D **13**, 459 (1991)
16. L. Lutterotti, P. Scardi, J. Appl. Crystallogr. **23**, 246 (1990)
17. J. Huot, S. Boily, E. Akiba, R. Schulz, J. Alloys Comp. **280**, 306 (1998)
18. A. Bassetti, E. Bonetti, A.L. Fiorini, J. Grboviæ, A. Montone, L. Pasquini, M. Vittori Antisari, Mat. Sci. Forum **453-454**, 205 (2004)
19. A. Zaluska, A. Zaluski, J.O. Ström-Olsen, Appl. Phys. A **72**, 157 (2001)
20. M.T. Hagström, P.D. Lund, Thermochimica Acta **298**, 141 (1997)
21. G. Barkhordarian, T. Klassen, R. Bormann, J. Alloys Comp. **364**, 242 (2004)
22. S. Dal Toè, S. Lo Russo, A. Maddalena, G. Principi, A. Saber, S. Sartori, T. Spataru, Mater. Sci. Eng. B **108**, 24 (2004)